Size effect in porous microbeams: Analytical solutions based on modified strain gradient theory

José Barbosa do Nascimento Neto[1], Fabio Carlos da Rocha[1]

[1]*Dept. of Civil Engineering, Federal University of Sergipe*
Av. Marcelo Deda Chagas, 49107-230, São Cristovão - SE, Brazil
bosinha89@academico.ufs.br, fabiocrocha@academico.ufs.br

Abstract. Micro/nano-scale beams, such as micro-electromechanical systems, micro actuators, and nanocomposites, are essential in engineering applications. However, classical elasticity theory fails to predict their mechanical behavior accurately due to the pronounced size effects at small scales. To address this limitation, the modified strain gradient theory (MSGT) introduces an additional equilibrium equation and incorporates five elastic constants (three non-classical and two classical) to better capture microstructural phenomena in isotropic linear elastic materials. This work develops analytical solutions for porous microbeams based on MSGT, considering various boundary conditions and four different porosity models. The results provide a more accurate framework for analyzing the mechanical behavior of micro-scale porous structures.

Keywords: Micro/nano-scale beams, analytical solutions, modified strain gradient theory, porosity models, various boundary conditions.

1 Introduction

Many porous structures exist in nature, including honeycomb-like material and foam-like structures such as bone, plant parenchyma, and sponges. These materials exhibit good strength-to-weight ratios, high energy absorption capacity, and low density. Owing to these properties, such structures have been extensively applied in various engineering fields, particularly in microscale-related problems, such as micro/nano electromechanical devices (MEMS and NEMS), thin films, sensors, and actuators. However, in microscale applications, classical elasticity theories become inadequate for capturing size-dependent effects. The Modified Strain Gradient Theory (MSGT), proposed by Lam et al. [1], becomes an alternative to overcome the limitations of classical elasticity theory by incorporating higher-order internal length scale parameters.

Within the framework of microstructural theories, several studies have applied MSGT to Euler–Bernoulli (EB) microbeams. For example, Kahrobaiyan et al. [2] modeled functionally graded (FG) beams under bending and vibration, while Li et al. [3] investigated static bending using different nonlocal models. Regarding porous functionally graded structures, Karamanli et al. [4] and Nguyen et al. [5] applied MSGT to metal foam microbeams with variable porosity. Wang et al. [6] conducted vibration and bending analyses on porous microbeams using MSGT, and Nguyen et al. [7] employed the Modified Couple Stress Theory (MCST) to study buckling, bending, and free vibration of porous microbeams under various boundary conditions.

Despite these advancements, an exact analytical approach for the analysis of functionally graded porous microbeams is still lacking in the literature. Therefore, the present work proposes closed-form analytical solutions, based on the MSGT, to investigate the static behavior of microbeams with a foam matrix. Addressing this gap is essential given the high potential of foams for applications in advanced microstructured systems.

2 Formulation

2.1 Functionally graded metal foam microbeam

Figure 1 shows a metal foam microbeam with length *L*, height *h*, and width *b*, and illustrates the pore distribution models: non-uniform porosity 1 (NUPD 1), non-uniform porosity 2 (NUPD 2), non-uniform porosity 3 (NUPD 3) and uniform porosity (UPD). The material properties vary along the height direction *h* of the microbeam. Furthermore, the Young's modulus *E*, shear modulus *G*, and mass density ρ of the metal foams are described by eq. (1) [2]:

$$E\ z\ = E_m\left[1-e_0\lambda(z)\right],\ G(z)=G_m\left[1-e_0\lambda(z)\right],\ \rho(z)=\rho_m\left[1-e_0\lambda(z)\right]. \tag{1}$$

Where $\lambda(z)=\cos\ \pi z/h$, $\lambda(z)=1-\cos\ \pi z/h$ and $\lambda(z)=\cos\ \pi z/(2h)+\pi/4$ correspond to the porosity distribution models NUPD1, NUPD2, and NUPD3, respectively. For the UPD model, $\lambda(z)=\alpha$ to describe both Young's modulus and shear modulus, while for the mass density $\lambda(z)=\alpha'$.

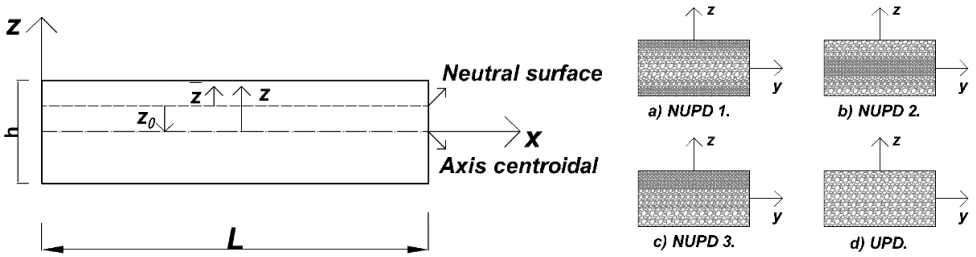


Figure 1 - Metal foam microbeam.

2.2 Kinematics

From the Euler-Bernoulli beam theory and integrating eq. (2) with respect to z, the kinematic relation given in eq. (3) is obtained.

$$\gamma_{xy}=\partial u/\partial z+\partial w/\partial x=0. \tag{2}$$

$$u(x,z)=u_0(x)-(z-z_0)\,\partial w/\partial x, \tag{3}$$

where $u_0(x)$ is the displacement at the neutral surface and z_0 is the offset between the neutral axis and the centroidal. Assuming a linearly elastic material, small displacements, and the absence of axial resultant force, eq. (4) is obtained, which defines parameter z_0.

$$z_0=\int_A E(z)z\,dA\Big/\int_A E(z)\,dA. \tag{4}$$

The strain field is described by means of the modified strain gradient theory (Lam et al [3]), as presented in eqs. (5) and (6).

$$\varepsilon_{ij}=\frac{1}{2}\ u_{i,j}+u_{j,i}\ ,\ \chi^s_{ij}=\frac{1}{2}\ e_{ipq}\varepsilon_{qj,p}+e_{jpq}\varepsilon_{qi,p}\ ,\ \gamma_i=\varepsilon_{mm,i}. \tag{5}$$

$$\eta^{(1)}_{ijk}=\frac{1}{3}\ \varepsilon_{jk,i}+\varepsilon_{ki,j}+\varepsilon_{ij,k}\ -\frac{1}{15}\delta_{ij}\ \varepsilon_{mm,k}+2\varepsilon_{mk,m}\ -\frac{1}{15}\left[\delta_{jk}\ \varepsilon_{mm,i}+2\varepsilon_{mi,m}\ +\delta_{ki}\ \varepsilon_{mm,j}+2\varepsilon_{mj,m}\ \right] \tag{6}$$

Where ε_{ij} is the strain tensor, $u_{i,j}$ is the derivative of the displacement vector, $\varepsilon_{mm,i}$ is the dilation gradient vector, $\eta^{(1)}_{ijk}$ is the symmetric part of the high-order strain gradient tensor, δ_{ij} is the Kronecker delta, χ^s_{ij} is the symmetric rotation gradient tensor, and e_{ijk} is the permutation symbol. The components of the Cauchy stress tensor σ_{ij}, as well as the high-order stress tensors p_i, $\tau^{(1)}_{ijk}$, and m^s_{ij}. are expressed in eq. (7).

$$\sigma_{ij} = k\delta_{ij}\varepsilon_{mm} + 2\mu\varepsilon_{ij},\ p_i = 2\mu l_0^2\gamma_i,\ \tau_{ijk}^{(1)} = 2\mu l_1^2\eta_{ijk}^{(1)},\ m_{ij}^s = 2\mu l_2^2\chi_{ij}^s. \tag{7}$$

Where k is the bulk modulus, l_0, l_1 and l_2 are the scale length parameters and μ the shear modulus.

2.3 Governing equations and boundary conditions

The strain energy U and the energy due to external forces W are described in eq. (8).

$$U = \frac{1}{2}\int_V \sigma_{ij}\varepsilon_{ij} + p_i\gamma_i + \tau_{ijk}^{(1)}\eta_{ijk}^{(1)} + m_{ij}^s\chi_{ij}^s\ dV,\ W = -\int_0^L q_w w(x)dx \tag{8}$$

To determine the strain fields, eq. (3) was applied to eq. (5) and eq.(6) to obtain the strain components. These components were then substituted into eq. (7) to establish the relationships between the stress tensors. Subsequently, these expressions were applied to eq. (8). Form this equation, the principle of minimum potential energy and the variational calculus lemma were applied to derive the Euler equations presented in eqs. (9) and (10).

$$\delta w_0\colon\ \left[A_1 w_0^{(6)} - A_5 w_0^{(4)} - q(x)\right] = 0, \tag{9}$$

$$\delta w_0\colon\ \left[-A_1 w_0^{(5)} + A_5 w_0''' - Q(x)\right] = 0,\ \delta w_0'\colon\ \left[A_1 w_0'' - A_5 w_0^{(4)} - M(x)\right] = 0,\ \delta w_0''\colon\ \left[A_5 w_0''' - \tilde{M}(x)\right] = 0. \tag{10}$$

Where A_1 and A_5 are constants described in eq. (11) and Q, M and $\tilde{M}$ are, respectively, the shear force, the classical moment and the non-classical moment.

$$\begin{aligned} A_1 &= \int_A \left(E'(z)\ \left(z - z_0\right)^2 + 2\mu(z)l_0^2 + \frac{8}{15}\mu(z)l_1^2 + \mu(z)l_2^2 \right) dA, \\ A_5 &= \int_A \left(2\mu(z)l_0^2\ \left(z - z_0\right)^2 + \frac{4}{5}\mu(z)l_1^2\ \left(z - z_0\right)^2 \right) dA. \end{aligned} \tag{11}$$

2.4 Analytical solution

The general solution of eq. (9) consists of the sum of a particular solution and a homogeneous solution. Therefore, for a uniformly distributed load $q(x) = q$, the general equation is expressed in eq. (12):

$$w_0(x) = qx^4 \Big/ 24A_1 + C_1 + C_2 x + C_3 x^2 + C_4 x^3 + C_5 e^{\sqrt{A_1/A_5}\,L} + C_6 e^{-\sqrt{A_1/A_5}\,L}. \tag{12}$$

Where C_1, C_2, C_3, C_4, C_5 and C_6 are integration constants determined from the boundary conditions. The boundary conditions are as follows: for a simply supported beam (S-S) are $w_0(0) = w_0(L) = 0$, $M(0) = M(L) = 0$ and $\tilde{M}(0) = \tilde{M}(L) = 0$; for a clamped-free beam (C-F) are $w_0(0) = w_0'(0) = 0$, $w_0''(0) = w_0'''(L) = 0$ and $Q(L) = M(L) = 0$; for a clamped-supported beam (C-S) are $w_0(0) = w_0(L) = w_0'(0) = 0$, $w_0''(0) = w_0''(L) = 0$ and $-A_5 w_0^{(4)}(L) + A_1 w_0''(L) = 0$; and for a clamped-clamped beam (C-C) are $w_0(0) = w_0(L) = w_0'(0) = w_0'(L) = 0$ and $w_0''(0) = w_0''(L) = 0$.

3 Results and Discussion

Consider a beam with length $L = 20h$, height h, and width $b = 2h$, subjected to a uniformly distributed load $q = 10\mu N/\mu m$. The materials properties are assumed to be $E_m = 200GPa$, $\rho_m = 7850kg/m^3$, $\nu_m = 0.33$, representing the Young's modulus, the mass density and the Poisson's ratio of the matrix, respectively. For simplification, it is assumed that the three material length scale parameters are equal to l, and the dimensionless deflection is expressed as $w = 1000w_0E_m bh^3/(12qL^4)$. Figure 2 shows the dimensionless maximum deflection as

a function of the porosity index e_0 , ranging from 0 to 0.9, for two cases: (a) $h = l$ and (b) $h = 5l$.

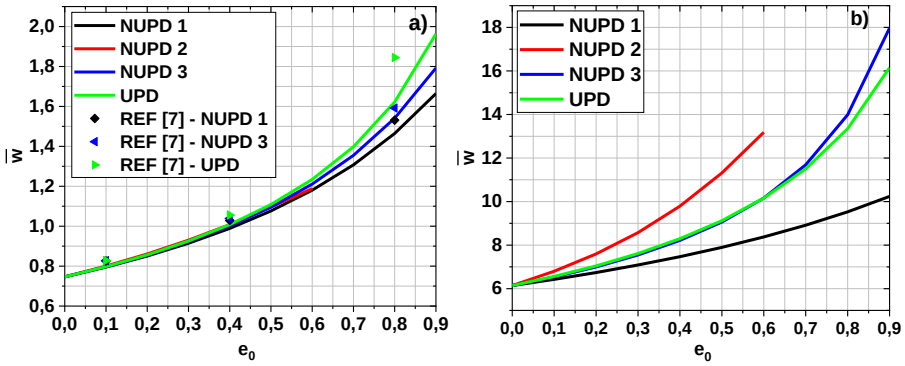


Figure 2 - Dimensionless deflection vs. porosity index of a simply supported microbeam: (a) $h = l$. (b) $h = 5l$.

Figure 2(a) shows that, for low porosity indices, the different porosity distribution models do not exhibit significant variations. However, as the porosity index increases, particularly for values above 0.6, more noticeable differences in deflections appear, highlighting the influence of the porosity model on the structural response. In addition, the proposed model demonstrates good accuracy when compared with the results reported by Nguyen et al. [7].

In Figure 2(b), for h = 5l , discrepancies among the models are already observed even for lower porosity indices, indicating that the structural scale directly affects the mechanical behavior, thus emphasizing the size effect. In comparative terms, the NUPD 1 model yields the lowest deflections among the evaluated models. Figure 3(a)-(d) present the dimensionless maximum deflections for various boundary conditions and *h/l* ratios, considering a porosity index of e_0 = 0.6 and the NUPD 1 distribution model. It is observed that both the boundary condition and the *h/l* ratio significantly influence the structural response. In general, as the h/l ratio increases, the deflections also increase. This behavior occurs because size effects become less relevant as the beam height *h* becomes much larger than the material's intrinsic length scale parameter *l*, causing the response to approach that predicted by classical elasticity theory. Regarding the boundary conditions, the structural response is strongly affected by the type of support. The clamped-free (C-F) configuration, which imposes the least restriction on movement, exhibits the largest displacements, especially at the free end. In contrast, the clamped-clamped (C-C) configuration shows the lowest deflections, as it imposes greater constraints on displacements and rotations.

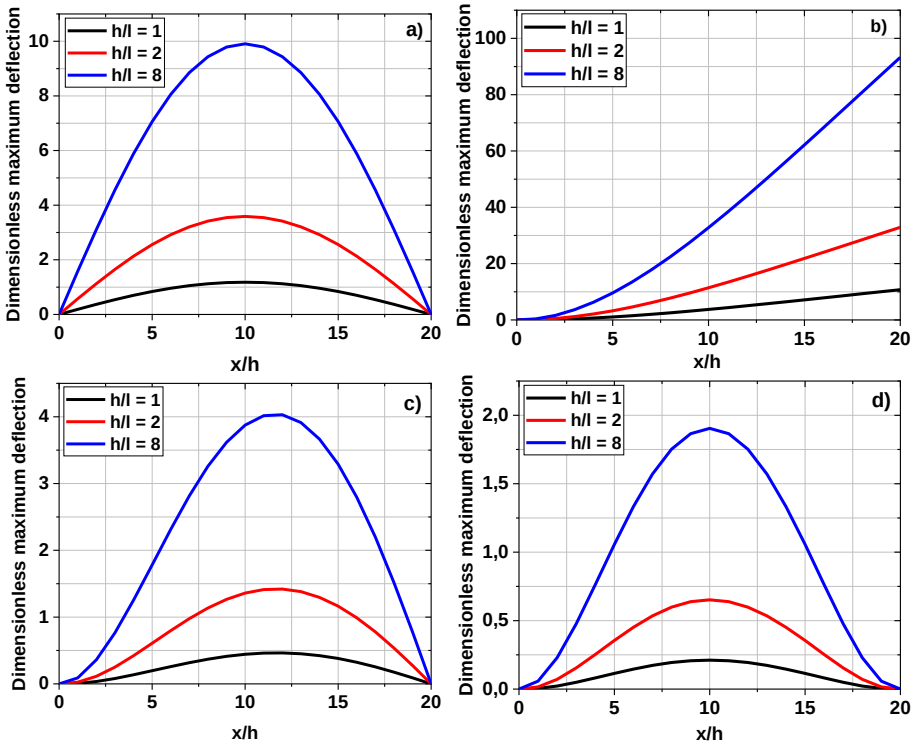


Figure 3 - Dimensionless maximum deflections (NUPD 1 with porosity 0.6) for: a) S-S. b) C-F. c) C-S. d) C-C.

4 Conclusions

This study analyzed the mechanical behavior of porous microbeams using the MSGT through an analytical approach under various boundary conditions. The results indicate that, for low thickness-to-material length scale rations (*h/l)*, a regime where size effects are more pronounced, and low porosity indices, the influence of the porosity distribution model is relatively limited.

It was also observed that boundary conditions significantly affect the displacement fields: configurations with lower constraint, such as clamped-free, lead to larger deflections, especially at the free end, while more restrictive conditions, such as clamped-clamped, result in smaller displacements due to the increased imposed stiffness.

Furthermore, the findings demonstrate that MSGT effectively captures scale-dependent behavior and accurately describes the mechanical response of micro-scale structures, where classical elasticity theory becomes inadequate.

The main contribution of this work lies in the development of analytical solutions based on MSGT, reinforcing the importance of generalized continuum models in the analysis of small-scale structural systems.

Acknowledgements. J.B.N.N and F.C.R would like to thank FAPITEC/SE. J.B.N.N acknowledges the scientific initiation scholarships granted, and F.C.R. acknowledges the financial support received through the Universal Project No 019203.01702/2024-6 and from FAPITEC/SE/FUNTEC-PRAPEC (Call No 05/2025).

Authorship statement. The authors hereby confirm that they are the sole liable persons responsible for the authorship of this work, and that all material that has been herein included as part of the present paper is either the property (and authorship) of the authors, or has the permission of the owners to be included here.

References

[1] D. C. C. Lam, F. Yang, A. C. M. Chong, J. Wang, and P. Tong, "Experiments and theory in strain gradient elasticity," *J Mech Phys Solids*, vol. 51, no. 8, pp. 1477–1508, Aug. 2003, doi: 10.1016/S0022-5096(03)00053-X.

[2] M. H. Kahrobaiyan, M. Rahaeifard, S. A. Tajalli, and M. T. Ahmadian, "A strain gradient functionally graded Euler-Bernoulli beam formulation," *Int J Eng Sci*, vol. 52, pp. 65–76, Mar. 2012, doi: 10.1016/j.ijengsci.2011.11.010.

[3] C. Li, H. Qing, and C.-F. Gao, "Theoretical analysis for static bending of Euler–Bernoulli using different nonlocal gradient models," *Mechanics of Advanced Materials and Structures*, vol. 28, no. 19, pp. 1965–1977, 2021, doi: 10.1080/15376494.2020.1716121.

[4] A. Karamanli, T. P. Vo, and O. Civalek, "Finite element formulation of metal foam microbeams via modified strain gradient theory," *Eng Comput*, vol. 39, no. 1, pp. 751–772, Feb. 2023, doi: 10.1007/s00366-022-01666-x.

[5] N. D. Nguyen, T. N. Nguyen, T. K. Nguyen, and T. P. Vo, "A Chebyshev–Ritz solution for size-dependent analysis of the porous microbeams with various boundary conditions," *International Journal of Mechanics and Materials in Design*, vol. 19, no. 4, pp. 861–881, Dec. 2023, doi: 10.1007/s10999-023-09666-5.

[6] Y. Q. Wang, H. L. Zhao, C. Ye, and J. W. Zu, "A porous microbeam model for bending and vibration analysis based on the sinusoidal beam theory and modified strain gradient theory," *Int J Appl Mech*, vol. 10, no. 5, Jun. 2018, doi: 10.1142/S175882511850059X.

[7] N. D. Nguyen, V. T. Bui, and T. K. Nguyen, "A modified strain gradient theory for buckling, bending and free vibration behaviors of metal foam microbeams," *Structures*, vol. 64, Jun. 2024, doi: 10.1016/j.istruc.2024.106533.

[8] J. Yang, D. Chen, and S. Kitipornchai, "Buckling and free vibration analyses of functionally graded graphene reinforced porous nanocomposite plates based on Chebyshev-Ritz method," *Compos Struct*, vol. 193, pp. 281–294, Jun. 2018, doi: 10.1016/j.compstruct.2018.03.090.